Boundary Layer in a High Current Density Discharge

Claudio G. Parazzoli*
Northrop Corporation, Hawthorne, Calif.

A high current density discharge can be, under proper conditions, established between the top and the bottom of a supersonic flow channel with a rectangular cross section. In proximity of the negatively biased electrode, the cathode, large potential gradients arise, and a considerable amount of heat is dissipated in the boundary-layer flow. A compression fan has been observed emanating from the leading edge of the cathode. A numerical and experimental investigation of this phenomenon is the subject of this paper. The density distribution in the boundary layer over the cathode, in the presence of the electrical discharge, has been measured and compared with the theoretical predictions. Also, the strength of the perturbation emanating from the cathode leading edge has been measured and calculated.

Introduction

IN certain categories of high-power electrically excited gas lasers, the mixture flows through a two-dimensional supersonic nozzle. The lasing region is located downstream of the nozzle where the flow Mach number is approximately 3.0-4.0, and the state density is of the order of ρ_s.†

A high D.C. voltage (2-5 kV) is applied perpendicularly to the flow, and a discharge established, in the region where the optical power is to be extracted. The electrical discharge, with current density $J \sim 0.1\text{-}1.0$ A/cm^2, is stablized by means of an electron beam whose electrons have an energy of approximately 150 keV.

Under the conditions described, a large potential gradient is established in proximity of the cathode. This region is usually referred to as the "cathode fall region." Due to the strong potential drop in the vicinity of the cathode, large electric fields are generated. consequently, a substantial amount of power $(E \cdot J)$ is deposited in the boundary layer next to the cathode. Most of this power appears as heat addition which changes the growth rate of the boundary layer. This in turn produces a disturbance, emanating from the leading edge of the cathode, which propagates into the core flow. Due to the stringent requirements of the gas homogeneity for good optical quality in large gas lasers, the estimate of the magnitude of the flow disturbance and its eventual compensation are of vital importance for a laser cavity design. In this research, a reliable numerical code to predict the effect of the cathode fall on the growth rate of the boundary layer was developed. The experiments performed have confirmed the predictions of the numerical calculations. The novelty of these calculations lies in the fact that for the first time the boundary-layer equations have been consistently solved in conjunction with the cathode fall equations. Moreover, the existence and magnitude of the cathode disturbance have been experimentally established.

Analytical Model

A. The Boundary-Layer Equations

The equations governing the flow of a compressible, turbulent two-dimensional boundary layer with heat addition, have been written in a form amenable to numerical calculations as suggested in Ref. 1. Also, allowance for variable specific heats has been made in view of the high temperatures expected in the boundary layer in connection with the large amount of heat released in it. The momentum equation is unchanged from Eq. (II-14) of Ref. 1. The energy equation (II-15) of Ref. 1 has been modified with the introduction in the right hand side of the nondimensional heat addition term

$$\delta^* \dot{Q}/\rho_e U(h_e^0 - h_r)$$

where δ^* is the boundary-layer displacement thickness, ρ_e, U, and h_e^0 are the freestream density, velocity, and stagnation enthalpy, respectively, and h_r is a reference enthalpy. For convenience of the reader, the momentum and energy equations, (II-14) and (II-15) of Ref. 1, are given below. The x axis is in the downstream direction and the y axis is normal to the bottom of the flow channel.

$$-\left\{\frac{\Upsilon}{d}[d(1-f')\right\}' + \left[(\eta - f)Q - \frac{\rho_w v_w}{\rho_e U} - \delta^* f_x\right] df''$$

$$+\left\{\left[Q(\eta - f) - \frac{\rho_w v_w}{\rho_e U} - \delta^* f_x\right] \cdot d' - (2 - f')(dP + d_x \cdot \delta^*)\right\} f'$$

$$-\left[(\eta - f)Q - \frac{\rho_w v_w}{\rho_e U} - \delta^* f_x\right] d' + P(d-1) + d_x \delta^*$$

$$= (1 - f')\delta^* df_x' \tag{1}$$

$$\left[\frac{\Upsilon_g}{d}\left\{g'' - \frac{1}{H}\frac{\frac{\gamma_e - 1}{2}M_e^2}{1 + \frac{\gamma_e - 1}{2}M_e^2}\left(\frac{v_e}{v_{eg}} - 1\right)\right.\right.$$

$$\left.\left. \cdot \left[d^2(1-f')^2\right]'\right\}\right]' + g''\left[Q(\eta - f) - \delta^* f_x - \frac{\rho_w v_w}{\rho_e U}\right]$$

$$= (1 - f')\delta^* g_x' + \frac{\delta^* \dot{Q}}{\rho_e U(h_e^o - h_r)} \tag{2}$$

Equation (II-16) of Ref. 1, allowing for variable specific heats, becomes:

$$\frac{\rho_e}{\rho} = d = \left\{\left[(1 - g'H)\left(1 + \frac{\gamma_e - 1}{2}M_e^2\right) - 1\right.\right.$$

$$\left.\left. - \frac{\gamma_e - 1}{\gamma_e} I(d)\right] \Big/ \left[\frac{\gamma_e - 1}{2} M_e^2 \cdot (1 - f')^2\right]\right\}^{1/2} \tag{3}$$

Submitted Jan. 11, 1977; presented as Paper 77-64 at the AIAA 15th Aerospace Sciences Meeting, Los Angeles, Calif., Jan. 24-26, 1977; revision received March 18, 1977.

Index categories: Boundary Layers and Convective Heat Transfer—Turbulent; Lasers.

*Staff Member, Northrop Research and Technology Center.

†(ρ_s = standard density).

Where the f', g' have the usual definition:

$$f'(x,y) = \frac{\rho_e U(x) - \rho u(x,y)}{\rho_e U(x)}$$

$$g'(x,y) = \frac{h_e^o - h^o(x,y)}{h_e^o - h_r}$$

M_e, γ_e are the freestream Mach number and specific heat ratio, respectively. The $'$ indicates the differentiation respect to η, the subscript x the differentiation respect to x. $\eta = y/\delta^*$, ν_e and ν_{eg} the effective viscosity and heat conductivity; $\Upsilon = \nu_e/U\delta^*$, $\Upsilon_g = \nu_{eg}/U\delta^*$ normalized effective viscosity and conductivity;

$$Q = (\rho_e U\delta^*)_x/\rho_e U; \quad P = \delta^* U_x/U$$

$I(d)$ is the integral involving the local specific heat ratio γ:

$$I(d) = \int_1^d \frac{\gamma(x)}{\gamma(x)-1}\,dx$$

with $x = \rho_e/\rho$. It has been assumed that the same form of the effective viscosity and heat conductivity can be used as for a turbulent boundary layer without heat addition.[1] This assumption has been necessary for lack of any experimental data relating to our particular phenomenon.

B. The Plasma Equations in the Cathode Fall Region‡

The mixture of gases, in which several singly ionized species and electrons are present, has been considered. The gradients normal to the cathode have been assumed much larger than those parallel to it, thereby reducing the problem to one dimension.

The following sign conventions for the various components of the electric current are used. The current density of the positive (negative) ith ions specie is given by:

$$J_{\mp i} = \mp \frac{E}{|E|} n_{\mp i} e v_{\mp i}$$

The electron current density is:

$$j_{-e} = -\frac{E}{|E|} n_{-e} e v_{-e}$$

Where $n_{\mp i}$ and n_{-e}, $v_{\mp i}$ and v_{-e} are the number of densities and magnitude of the drift velocities for ions and electrons, respectively, e is the magnitude of the electronic charge. E is the electric field. The total current density is:

$$J = \sum_{i=1}^{n} (J_{+i} - J_{-i}) - J_{-e}$$

The weakly ionized plasma in the cathode fall region can be described completely by the Poisson equation and the continuity equation for the ionic species and for the electrons. For the ion and electron velocities we used the drift velocities as in Refs. 2 and 3. The momentum equations for the ions or the electrons have not been solved. A numerical example justifying this approach in our calculations is given in Ref. 4. In terms of the ion and electron current densities and drift velocities, the Poisson equation becomes:

$$\frac{dE}{dy} = +4\pi \frac{E}{|E|}\left[\sum_{i=1}^{n} \cdot \left(\frac{J_{+i}}{v_{+i}} + \frac{J_{-i}}{v_{-i}}\right) + \frac{J_{-e}}{v_{-e}}\right] \tag{4}$$

‡The CGS system of units is consistently used throughout this paper unless otherwise noted.

The continuity equations for $J_{\mp i}$ and J_{-e} are:

$$\frac{d}{dy}J_{+i} = eS_{T_i} + eS_{E_i} + \frac{\alpha_i}{e}\frac{J_{-e}}{v_{-e}}\frac{J_{+i}}{v_{+i}} - \frac{J_{+i}}{v_{+i}}\frac{E}{|E|}$$

$$\cdot N\sum_{\substack{j=1\\ j\neq i}}^{n} C_{ij}x_j + \frac{E}{|E|}Nx_i\sum_{\substack{j=1\\ j\neq i}}^{n} C_{ji}\frac{J_{+j}}{v_{+j}} \tag{5}$$

$$\frac{d}{dy}J_{-i} = -\frac{E}{|E|}\frac{J_{-e}}{v_{-e}}\beta_i \tag{6}$$

$$\frac{d}{dy}J_{-e} = e_{S_T} + eS_E + \frac{J_{-e}}{v_{-e}} \cdot \sum_{i=1}^{n}\frac{\alpha_i}{e}\frac{J_{+i}}{v_{+i}} + \frac{E}{|E|}\frac{J_{-e}}{v_{-e}}\sum_{i=1}^{n}\frac{\beta_i}{e} \tag{7}$$

where: n is the total number of components of the gas mixture; N is the number density of neutral particles; S_{Ti} is the ion generation rate due to the Townsend ionization; S_{Ei} is the ion generation rate due to the E-beam ionization; and α_i/e, $J_{-e}/v_{-e}\,J_{+i}/v_{+i}$ is the ion loss rate due to recombination.

The last two terms on the right hand side of Eq. (5) give the contribution of the charge exchange to the positive ith specie ions net generation rate.

C_{ij} are the charge exchange coefficients. β_i is the electron attachment coefficient to neutrals of the specie. x_i is the mole fraction of the ith specie.

In Eq. (7), S_T and S_E are the electron generation rate due to Townsend and E-beam ionization, respectively. Equations (4) through (7) constitute a system of 2 $(n+1)$ first-order differential equations in 2 $(n+1)$ unknowns. The system can be properly integrated when the neutral particle density distribution $N = N(y)$ through the cathode fall region is specified. A detailed derivation of S_{Ti}, S_{Ei}, S_T, and S_E is given in Ref. 4.

Initial Conditions

At the cathode we assume $J_{-i}(0) = 0$, because very little electron attachment can take place there. For the case of a single gas component mixture, the initial conditions for the ion and electron current densities are:

$$J_+(0) = \frac{J + J_o}{\gamma_i + 1}$$

and

$$J_{-e}(0) = \frac{J_o - \gamma_i J}{\gamma_i + 1}$$

where γ_i is the secondary electron emission coefficient (number of electrons emitted per ion impinging on the cathode surface) and J_o is the photo current.

For a multispecies gas mixture, the initial conditions are stated below without justification. The interested reader is referred to Ref. 4 for details of the derivation. At

$$y = 0: \tag{8a}$$

$$J_{-i}(0) = 0 \tag{8b}$$

$$J_{+i}(0) = \kappa v_{+i}\left[\frac{f_i}{e}\alpha_T(0)J_{-e}(0) + S_{Ei}\right]\frac{E}{|E|} \tag{9}$$

where

$$f_i = \frac{x_i Q_i}{\sum_{j=1}^{n} x_j Q_j}$$

Q_i being the ionization cross section of the ith specie;

$$\kappa = \left[(J + J_o)E/|E|\right] \Big/ \left\{\sum_{1=i}^{n} v_{+i}\left(\frac{f_i}{e}\cdot\alpha_T(0)J_{-e}(0) + S_{Ei}(\gamma_i + 1)\right)\right\} \cdot J_{-e}(0) = \frac{-b - \sqrt{b^2 - 4ac}}{2a} \tag{10}$$

where

$$a=\sum_i -\frac{f_i}{e}\alpha_T(0)v_{+i}(\gamma_i+1) \tag{11a}$$

$$b=\sum_{i=1}^{n} v_{+i}\left[-S_{E_i}(\gamma_i+1)+\frac{f_i}{e}\alpha_T(0)(J_o-\gamma_i J)\right] \tag{11b}$$

$$c=\sum_i v_{+i}S_{E_i}(J_o-\gamma_i J) \tag{11c}$$

At $y=d_c$:

$$J_{-e}(d_c)\simeq -J$$

The system of Eqs. (4) through (7) has a total of 2 $(n+1)$ first-order ordinary differential equations. These differential equations require for their integration $2(n+1)$ boundary conditions which are supplied by Eqs. (8), (9) and (11). While for the system of Eqs. (4) through (7), as a whole, the initial boundary-value problem is well posed, this is not the case of each single differential equation. In particular, Eq. (4) for the electric field has no boundary conditions. In contrast, Eq. (7) for the electron current density J_{-e}, has two boundary conditions, which are too many for a first-order differential equation. This uneven distribution of the boundary conditions among the constituent equations of the system makes the process of numerical integration more time consuming because an iterative procedure is required.

The following iterative procedure is employed: a) An initial guess for the value of E field at $y=0$ is taken. Let $E_o^o<0$ be such a guess. b) The step-by-step numerical integration of the system of equations is then carried on until one of the following events occurs: 1) the E field becomes positive; or 2) the total positive ion current

$$\left(\sum_{i=1}^{n} J_{+i}\right) \text{ becomes greater than zero,}$$

which is concomitant with a reverse in the sign of dE/dy. c) A new guess value for E_o, let us say E_o^1, is then made, and a new numerical integration carried on. We choose $E_o^1<E_o^o$ $(E_o^1>E_o^o)$ if the calculation in b) were terminated because

$$E>0 \quad \left(\sum_{i=1}^{n} J_{+i}>0\right)$$

d) The procedure is repeated until $E_o^n-E_o^{n-1}\leq\epsilon$, where ϵ is a small arbitrary number. E_o^n and E_o^{n-1} are two values of the electric field at the cathode for which the respective integration is terminated because $E>0$ and

$$\sum_{i=1}^{n} J_{+i}>0$$

The y position at which the iteration is terminated is taken to be d_c, the cathode fall thickness. If ϵ is chosen small enough, say 10^{-3} E_o, the outer boundary conditions,[11] is satisfied within one percent (1%) or better. The values of current density J, and freestream density, of interest in our calculations, are $J\sim 0.1\text{-}1.0$ A/cm^2, $\rho_e\sim 0.1\text{-}1.0\ \rho_s$. Correspondingly, the cathode fall thickness d_c is of the order of 10^{-2} cm, and $E.\simeq 200\text{-}300$ stat-volt/cm. (1 stat-volt = 300 volts).

The underlying justification for the use of d_c as the cathode fall thickness is that in proximity of $y=d_c$, the field gradients become comparatively small; i.e., quasineutrality is reached. The quasineutrality condition is an indication that we emerged from the cathode fall region. This consideration is in agreement with the common criterion[3] employed in the literature. Elsewhere,[2] the numerical integrations have been carried out as far as the anode which was taken a few cm away from the cathode. These numerical integrations have been possible because the calculations concerned cases with very low current densities, such as $J=10^{-7}\text{-}10^{-4}$ A/cm^2. As the current density is increased to the order of 1 A/cm^2, the computations become extremely sensitive to the initial value of the electric field E_o. Typically, a change of $(\Delta E_0/E_o)\simeq 10^{-5}$ is sufficient to change considerably the y value at which E becomes positive or

$$\sum_{i-1}^{n} J_{+i}$$

becomes larger than zero.

Clearly, the computing time, to extend the calculations a few centimeters away from the cathode, then becomes excessive. Moreover, no further valuable information on the cathode fall region itself is gained from terminating the calculations at the anode.

Table 1 Input data of the sample case

Gas N_2	
$M = 3.525$	$\frac{dM}{dx}=0$
$P_o = 6.672\times 10^6$ dynes/cm^2	
$J\cdot = -1.0123\times 10^{-9}$ stat A/cm^2 (.337 A/cm^2)	$dP_o/dx=0$
$\gamma_{N_2} = .06$	$T_o = 300$ K
$J_o = 3\times 10^3$ stat A/cm^2	
$\xi = 0$	

Combined Solution of the Boundary-Layer Equations and Cathode Fall Equations

To integrate the boundary-layer system of Eqs. (1-3), $\dot{Q}(y)=J\cdot E$ must be known. For a gas mixture of n components, $\dot{Q}$ is given by

$$\dot{Q}(y)=|E\sum_{i=1}^{n} J_{+i}|+|E\sum_{i=1}^{n} J_{-i}|+|EJ_{-e}|\xi \tag{12}$$

In Eq. (12), it has been assumed that all the energy acquired by the ions in the discharge is transferred without delay to the flow where it will appear in the form of heat. This assumption is justified in view of the fast relaxation times between the translational degree of freedom of the ions and neutrals. The electrons, in the collisions with the gas neutrals, transfer a large part of the energy lost in the impact to degrees of freedom of the neutral atoms and molecules other than the translational ones. Namely, the electrons ionize gas molecules and excite electronic vibrational levels in atoms and molecules. Therefore, it is reasonable to assume that only a fraction ξ of the electron energy appears immediately as heat in the boundary-layer flow.

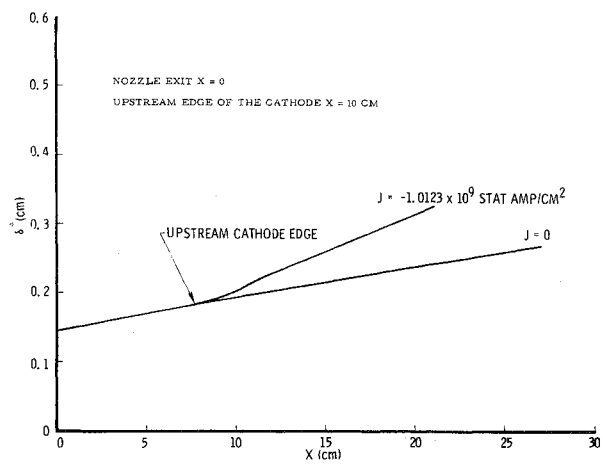

Fig. 1 Sample case, displacement thickness (δ^*) vs X.

Estimation of this fraction ξ is not easily done. However, as the results of the calculations will prove, the energy deposited by the discharge in the electrons is small compared to the energy deposited in the ions. Hence, whatever value of $\xi(0<\xi<1)$ we may choose, the results of the calculations will not be greatly affected. That is, almost the entire input power to the cathode fall region is converted to heat.

The system of the boundary-layer equations (1-3) and the system of the cathode fall Eqs. (4-7) are linked by $\dot{Q}$ and E/N, where $\dot{Q}$ is the power per unit volume dissipated in the flow by the discharge. Our numerical code solves consistently the set of Eqs. (1) through (7).

Results of the Numerical Calculations

The results of the numerical calculations for a sample case are reported below for subsequent comparison with the experimental measurements. In Table 1 we listed the basic parameters for the sample case.

In Fig. 1, the displacement thickness δ^* is plotted vs x, coordinate in the flow direction, for the no discharge case ($J=0$), and $J=-1.0123\times10^9$ stat A/cm^2. In all of the calculations presented, the supersonic nozzle exit is at $x=0$ and the leading edge of the cathode is at 10 cm. The slope of δ^* changes corresponding with the beginning of the cathode. In the $J=0$ case, $d\delta^*/dx$ is 5.14×10^{-3}; when the discharge is present, $d\delta^*/dx$ increases to 9.22×10^{-3}.

In Fig. 2, ρ_e/ρ is plotted vs y/δ^*, the normalized distance from the cathode, for different values of x. As a comparison, ρ_e/ρ vs y/δ^* is shown for the no discharge case as well. For the $J=0$ case, there is no detectable dependence on x of the ρ_e/ρ vs y/δ^* profiles. (Note that the value of δ^* is different with an without discharge.) With a discharge, the maximum value of ρ_e/ρ is achieved in proximity of the wall, typically for $y/\delta^*=2\times10^{-2}$ which corresponds to $y=5\times10^{-3}$ cm.

In Fig. 3, the power in the ion mode $P_{\text{ion}}=|E\cdot J_{+i}|$ and the power in the electron mode, $P_{\text{elc}}=|E\cdot J_{-e}|$ are plotted as a function of y/δ^* at three x positions. P_{ion} is a monotonic decreasing function of y/δ^*. P_{elc} instead presents a rather flat maximum. From the kinetic of the discharge, it is reasonable to assume that only $\simeq 0.1\ P_{\text{elc}}$ appears directly as heat in the boundary layer. Therefore, the electron heating can be neglected for all the practical purposes. The three different curves for P_{ion} shown in Fig. 3 can be collapsed very nearly in a single one if P_{ion} is plotted vs y. This indicates that the cathode fall thickness d_c is very closely a constant along the surface of the cathode. For the case under consideration, $d_c\simeq 9.8\times10^{-3}$ cm.

Figure 4 shows the potential distribution in the cathode fall region. V (volts) is plotted as a function of y/δ^* at three x positions. The cathode fall $V_c=V(d_c)$ is a fairly weak function of x, $V_c\simeq 297$ V.

In Ref. 4, the effects on the boundary-layer growth and its internal structure of the current density J, of the secondary electron emission coefficient γ_i, and the stagnation pressure P_0 are shown in detail.

Experimental Results and Comparison with Theoretical Predictions

The section gives a description of the experimental apparatus used and of the measurements performed, and compares the theoretical calculations with the measured density changes in the flow, which are due to the heat addition in the cathode fall.

Figure 5 shows a top view of the experimental setup employed. The Ludwieg tube (LT), feeding into the two-dimensional supersonic nozzle (SN), provides a flow at $M=3.5$ in the channel (C), for the duration of 10-15 ms. In the flow channel C, and E-beam sustained electrical discharge is generated. Coincident with the discharge region, there are two (6×23 cm) viewing glass windows in the sidewalls of the channel. The channel width at this point is 25 cm and the channel height 6.0 cm. Interferograms of the flow are taken through the viewing windows according to the scheme shown in Fig. 5. The interferometer used is of the Twyman-Green variety. The interferometer consists of a ruby laser (L_1), along with an HeNe laser (L_2) used for alignment purposes; an expanding (negative) lens E_L; a beam splitter BS and the two reflecting mirrors M_1 and M_2; a focusing parabolic mirror M_{P2}; the electronic shutter S; and the photographic plate P.

The duration of the discharge and the timing of the laser pulse can be varied within reasonable limits. The length of the discharge is set between 200 and 500 μsec. The laser pulse

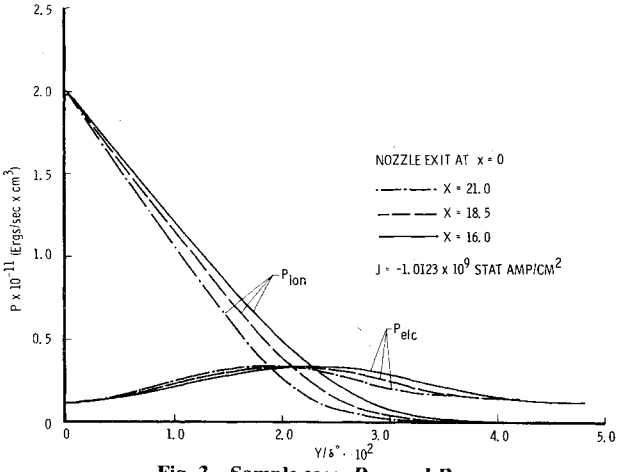

Fig. 3 Sample case, P_{ion} and P_{elc}.

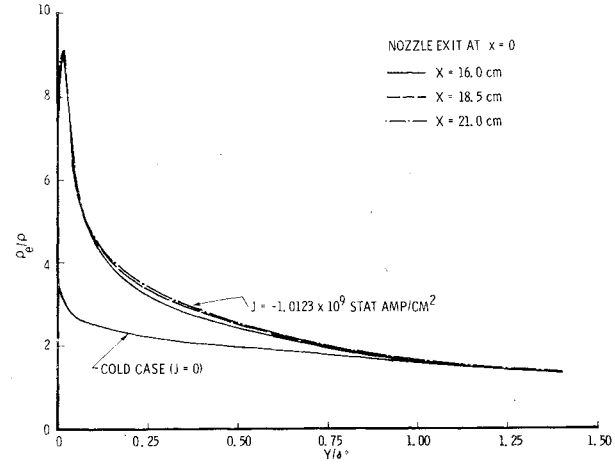

Fig. 2 Sample case, density profile in the boundary layer.

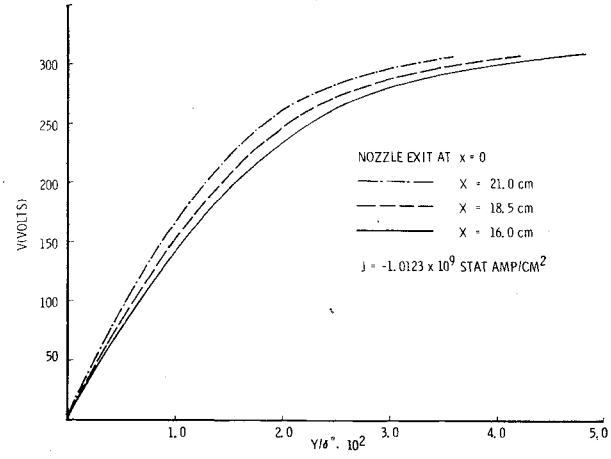

Fig. 4 Sample case, potential distribution.

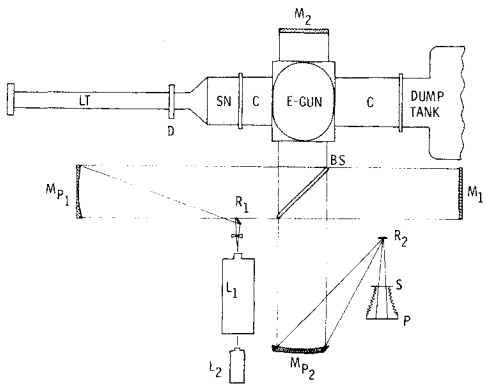

Fig. 5 Experimental apparatus. Legend: LT = Ludwieg tube, D = diaphragm, SN = two-dimensional supersonic nozzle, C = flow channel, L_1 = ruby laser, L_2 = HeNe laser, E_L = expanding lens, $R_{1,2}$ = plane reflecting mirror, $M_{P1,P2}$ 80″ focal length mirror, BS = beam splitter, $M_{1,2}$ = plane reflecting mirror, S = electronic shutter, P = photographic, w = channel width.

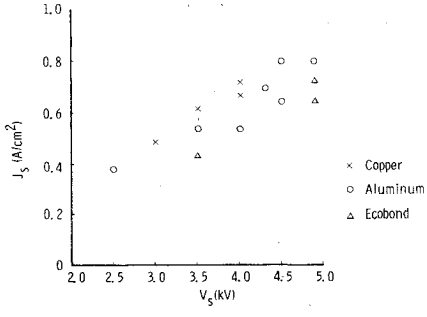

Fig. 6 Sustainer current density J_s as function of the sustainer voltage V_s for different cathode materials.

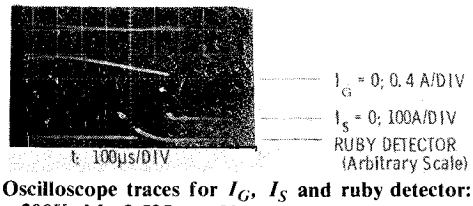

Fig. 7 Oscilloscope traces for I_G, I_S and ruby detector: $P_o = 6.8$ atm, $T_o = 300$K, $M = 3.525$, gas N_2, copper cathode, $V_s = 4.0$kV.

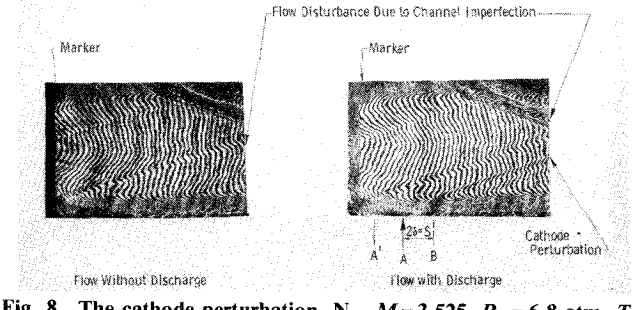

Fig. 8 The cathode perturbation. N_2, $M = 3.525$, $P_o = 6.8$ atm. $T_o = 300$ K, $V_s = 4.0$ kV, $J_s = 0.603$ amp/cm², picture scale = 0.9, $\Delta\rho/\rho$ % per fringe = 1.83.

normally is made to occur 50 μsec before the shutoff of the discharge. The sustainer voltages were varied between 2 and 5 kV; the electron beam energy is approximately 150 kV. The flow Mach number is 3.52, the gas used in N_2, the stagnation pressure and temperature in the Ludwieg tube are, respectively, 3-5 atm and 300K. The cathode and anode have a flow-wise length of 25 cm, and a width transverse to the flow of 15 cm. The cathode upstream edge is located 10 cm downstream from the end of the nozzle.

Experimental Results

In Fig. 6, the sustainer current density J_s is shown as a function of the sustainer voltage V_s for three different cathode materials. The difference in J_s for the three materials tested, C_u, Al and "Ecobond" (a conductive epoxy with a bulk resistivity of 25Ω/cm³) is not large but sufficient to establish that copper provides, for the same sustainer voltage V_s, a larger current density J_s than aluminum. Conversely, the "Ecobond" generates a sustainer current J_s somewhat smaller than aluminum.

Figure 7 shows the characteristic oscilloscope traces of the sustainer current I_s, E-gun current I_e, and the detector trace shows the time of firing of the ruby laser. Note the droop of I_s is due to the discharge of the capacitor bank and the droop in E-beam current.

Figure 8 shows two interferograms of the flow without discharge. In the interferogram taken during the discharge, the presence of the perturbation, emanating from the upstream edge of the cathode, is clear.

A direct linear extrapolation of the cathode perturbation through the boundary layer would intersect the wall at A'. Where A' is a point approximately 1.2 cm upstream from the cathode edge. However, to assume that the shock is emanating from A' would be erroneous because of the curvature of the Mach lines in the boundary layer.

Numerical calculations[4] have shown that: a) the Mach number in the boundary layer can be taken as a linear function of the distance from the wall; and b) the sonic line occurs very close to the wall. Hence, the Mach number in the boundary layer can be written as $M(\eta) = 1 + \eta\ (M_e - 1)$.

The charactteristic equation is then easily integrated throughout the boundary layer. As a result, the flow-wise separation s between the point A, where the perturbation meets the sonic line, and the point B, where it enters the boundary-layer region, is given by

$$s = \frac{\delta}{2(M_e - 1)}\left[M_e\sqrt{M_e^2 - 1} - \ell n\ (\sqrt{M_e^2 - 1} + M_e)\right]$$

For our conditions $M_e = 3.52$, hence $S = 1.97$. The numerical calculations set the sonic line in the boundary layer at approximately 10^{-2} cm from the wall. Finally, point A is found to be coincident with the upstream edge of the cathode. This proves that the observed perturbation is indeed emanating from the upstream edge of the cathode.

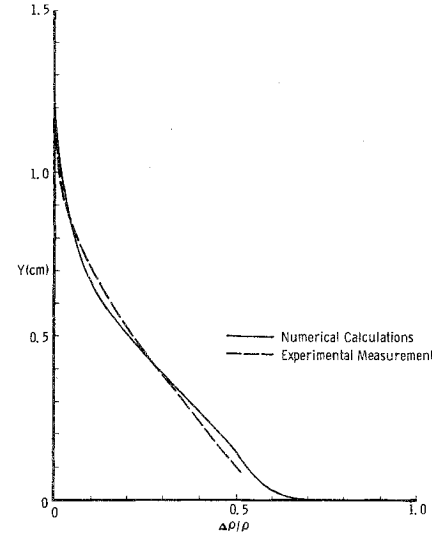

Fig. 9 Density profile in the boundary layer with no discharge N_2, $P_o = 6.8$ atm, $T_o = 300$ K, $M = 3.525$, distance from nozzle exit 34.9 cm.

Figure 9 offers a comparison between the interferometrically measured and calculated density profiles in the boundary layer for the case without discharge. In Fig. 10, the same comparison is made when the discharge is turned on.

The strength and detailed structure of the cathode perturbation are dependent on the rate of growth of δ^*, in the transition region between the plastic bottom of the channel and the metal edge of the cathode, and along the cathode. While we can compute with reasonable accuracy $d\delta^*/dx$ in the cathode region removed from the upstream edge, the same cannot be done for the transition region. In fact, in order to calculate δ^* we must know, or make reasonable assumptions, on the current density distribution J as a function of x. Clearly J can be considered a constant in the central region of the cathode. In the transition region we know that J must rapidly increase from zero to a reasonably constant value, but the details of this growth are not available at the present time.

A rough estimate of the strength of the perturbation can be made assuming that the flow would be similar to the one over a wedge with an angle equal to

$$tg^{-1}\left[\left(\frac{d\delta^*}{dx}\right)_{J_o}-\left(\frac{d\delta^*}{dx}\right)_{J_o=0}\right]$$

where J_o is the average value of J on the cathode. This assumption reflects the common practice of compensating the boundary-layer growth in a flow channel with a cross section increase proportional to the boundary-layer displacement thickness δ^*.

Figure 11 compares the calculated with the interferometrically measured density change across the cathode perturbation. Details on the data reduction process employed are given in Ref. 4.

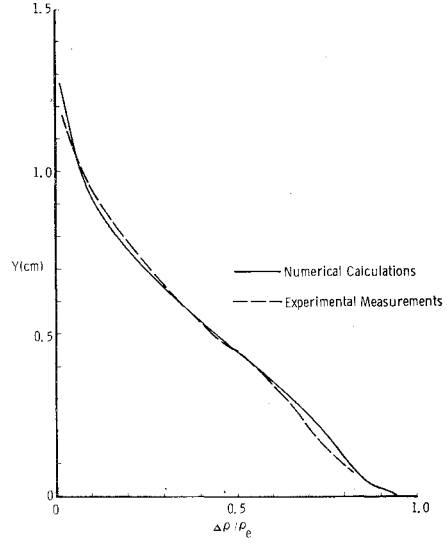

Fig. 10 Density profile in the boundary layer with discharge N_2, $P_o = 6.8$ atm, $T_o = 300$K, $M = 3.525$, $J = 0.629$ A/cm^2, distance from upstream edge of the cathode 24.9.

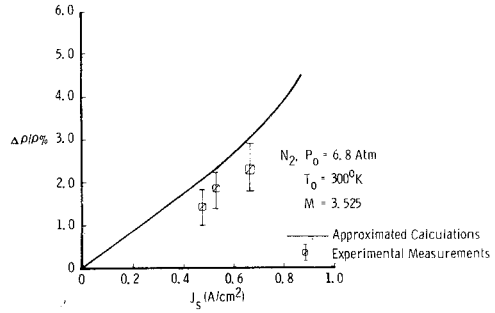

Fig. 11 Density changes across the cathode perturbation (approximated calculations) N_2, $P_o = 6.8$ atm, $T_o = 300$K, $M = 3.525$.

Conclusion

The results of this investigation can be summarized as follows: a) The numerical model developed, accurately predicts the effects of the cathode fall on the turbulent supersonic boundary layer. b) The perturbation produced in the flow outside the boundary layer by the change of growth rate of δ^*, can be estimated with reasonable accuracy, regardless of whether the details of $J = J(x)$ at the cathode leading edge are known. c) The cathode perturbation induces a density change $\Delta\rho/\rho$ in the core flow of the order of a few percent for sustainer current densities of the order of 1 A/cm^2.

Acknowledgments

I sincerely appreciate the support of Dr. B. B. O'Brien, whose discussion and criticism were essential to the development of this document. Also, special thanks to G. Duckworth for his help in programming and to D. Diem for his aid in the experimental investigations. This research was partially supported by ARPA and by the Air Force Weapons Laboratory, Kirtland Air Force Base, Albuquerque, New Mexico, Contract No. F29601-75-C-0018.

References

[1]Herring, H. J. and Mellor, G. L., "Computer Program for Calculating Laminar and Turbulent Boundary Layer Development in Compressible Flow," NASA CR-2068, June 1972.

[2]Ward, A. L., "Effect of Space Charge in Cold-Cathode Gas Discharges," *Physical Review*, Vol. 112, No. 6, Dec. 15, 1958, pp. 1852-1857.

[3]Ward, A. L., "Calculations of Cathode-Fall Characteristics," *Journal of Applied Physics*, Vol. 33, Sept. 1962, pp. 2789-2794.

[4]Parazzoli, C. G., Northrop Research and Technology Center, Hawthorne, Calif., June 1976.